Unsupervised Bushfire Burn Severity Mapping Using Aerial and Satellite Imagery

Ting Bai[1], Dominik Stütz[2], Chang Liu[1], Dimitri Bulatov[2], Jorg Hacker[3,4], Linlin Ge[1]

[1] School of Civil and Environmental Engineering, Faculty of Engineering, The University of New South Wales, Sydney, Australia - (ting.bai, chang.liu17, l.ge)@unsw.edu.au
[2] Fraunhofer IOSB, Ettlingen, Germany - (dominik.stuetz, dimitri.bulatov)@iosb.fraunhofer.de
[3] ARA-Airborne Research Australia, Adelaide, SA, Australia - jorg.hacker@airborneresearch.org.au
[4] College of Science and Engineering, Flinders University, Adelaide, SA, Australia - jorg.hacker@flinders.edu.au

Keywords: burned area mapping, LIDAR, aerial imagery, SAM, Style Transfer, biomass.

Abstract

It is critical to assess bushfire impact rapidly and accurately because bushfires play a significant role in forest degradation and present a threat to ecosystems and human lives. Over the past decades, several supervised algorithms of burn severity mapping have been proposed, facing the significant drawback of time-consuming labeling. Moreover, there is no robust framework for burn severity mapping through fusing multi-sensor, multi-resolution, and multi-temporal remote sensing imagery from satellite and aerial platforms. Therefore, this paper presents an unsupervised two-step pipeline: processing 2D data followed by 3D data for burn severity mapping, both of which are acquired from either aircraft or satellites. For the 2D data processing, our proposed unsupervised burned area detection (UsBA_detection) model enhances burned area mapping accuracy by integrating Ultra-High Resolution (UHR) aerial imagery with bi-temporal medium-resolution PlanetScope imagery, using a Segment Anything Model (SAM)-assisted UNetFormer (pre-trained on the target-style public dataset – LoveDA Rural) for refinement. The model demonstrates superior burned area segmentation, evidenced by improved evaluation metrics calculated from labeled test sites. For the 3D analysis, the burned areas extracted from 2D processing are further assessed using pre- and post-event airborne laser data. We implement a voxel-based workflow, including necessary steps such as ground filtering through Superpoints in RANSAC Planes (SiRP) method and biomass change analysis. The results indicate that the 3D branch provides a reliable lower bound of the actual damage map, because the vegetation growth between two measurements remains, in essence, undetected. The proposed framework offers a more accurate and robust solution for burn severity mapping utilizing combined 2D and 3D data, evaluated on a multi-source dataset from a real bushfire event that occurred in Bushland Park, South Australia.

1. Introduction

As the world’s climate changes and human activities expand, bushfires have become a more frequent and devastating reality, particularly in regions like Australia, where the ecological, societal, and economic impacts are profound (Sharples et al., 2016). Recent years have witnessed catastrophic bushfires, such as the 2019-2020 Australian bushfire season, also known as the “Black Summer”. The “Black Summer” alone resulted in the loss of over 33 lives, the destruction of more than 3,000 homes, and the burning of approximately 18.6 million hectares across the country (Davey and Sarre, 2020). Beyond the immediate loss of life and property, bushfires also lead to unprecedented burned areas, significant tree mortality, severe challenges for forest management, and extensive damage to ecosystems, exacerbating climate change.

While early prevention and identification of the fires is crucial, post-event accurate mapping of burned areas is equally vital for restoration activities (Chuvieco et al., 2019). The process of collecting ground-level data for accurate mapping, limited by the challenge of accessing vast and isolated areas impacted by wildfires, has proven to be slow and dangerous. Aerial or satellite platforms can solve this problem, providing us with moderate or high-resolution data for severity mapping, which allows us to extract the fire information remotely (Bai et al., 2023; Zhang et al., 2021). A lot of global-scale burned area products have been developed with the Moderate Resolution Imaging Spectroradiometer (MODIS) (Lizundia-Loiola et al., 2020). However, significant variations within small burned areas introduce mapping uncertainty with the limitations of coarse pixel spacing ($>250\,\mathrm{m}$). Then, the accuracies of these mapping products are increased with the launch of satellites such as Sentinel-2 and Landsat-8/9 based on medium spatial resolution images (Roteta et al., 2019; Roy et al., 2019). They provide the near-infrared (NIR) ($800\,\mathrm{nm}$ to $1200\,\mathrm{nm}$) and the short-wave infrared (SWIR) ($1200\,\mathrm{nm}$ to $2200\,\mathrm{nm}$) bands, which are highly sensitive to the fires. With the advent of daily accessible PlanetScope imagery from Planet Labs at better spatial resolution ($3\,\mathrm{m}$), there is now the capability to capture more detailed information before and after bushfires occur, demonstrating considerable promise for application in disaster management (Cho et al., 2022).

Alternatively, instruments such as visible, NIR, SWIR hyperspectral scanners, and light detection and ranging (LIDAR), installed on manned aircraft or unmanned aerial vehicles, have been employed to detail fire severity at the local scale (Arkin et al., 2019). Ultra-High Resolution (UHR) aerial imagery, offering detailed ground information, allows for visual interpretation and facilitates the manual or automatic identification of damaged objects affected by fires (McKenna et al., 2017). Depending on flight height and capability to penetrate through vegetation, the LIDAR data allows for biomass volume computation. However, two challenges are the volume of aerial data and its general lack of availability. High-resolution aerial imagery must be scheduled in advance and is typically only accessible after a bushfire event. In contrast, satellites equipped with medium-resolution sensors consistently capture the Earth’s surface, offering multi-temporal imagery for locations globally. Consequently, we find a research gap in that there is no ro-

This contribution has been peer-reviewed. The double-blind peer-review was conducted on the basis of the full paper.
https://doi.org/10.5194/isprs-annals-X-4-2024-29-2024 | © Author(s) 2024. CC BY 4.0 License.

bust framework developed specifically for efficiently detecting burned areas using aerial and satellite 2D optical images together with 3D LIDAR data.
The objective of this paper is to provide a comprehensive pipeline for analysis of 2D and 3D data without any annotated data. In 2D, we propose the UsBA detection model, an unsupervised approach for 2D burned area mapping. SAM-assisted UNetFormer (pre-trained on target-style LoveDA Rural Dataset) is employed to exclude water bodies and roads in burned area candidates, which are obtained from the combined use of aerial and satellite imagery. After detecting burned areas in 2D, the objective shifts to detect the burn severity by volume. Particularly, with these very task-specific categories of labels, it is highly non-trivial. This is where the sensor data function comes into play. We apply the voxel-based change detection module to the aforementioned clusters to separate the burned and unburned areas of the dataset. The crucial intermediate step for 3D analysis is to perform the ground filtering. This is done using the SiRP (Bulatov et al., 2020) method, which is particularly suitable for point clouds with explicit 3D structure.

2. Previous Works

2.1 Unsupervised Analysis of Optical Data

In recent years, machine learning (Ramo and Chuvieco, 2017; Gibson et al., 2020) and, particularly, deep learning (Belenguer-Plomer et al., 2021; Hu et al., 2023), have been widely used in burned area detection. Many of these approaches are supervised and depend on large volumes of manually labeled data for training. Unsupervised approaches offer a time-saving alternative that efficiently explores the patterns or structures of data. In burned area mapping, unsupervised Principal Component Analysis (PCA) is one of the most commonly used methods for the normalized burn ratio (NBR) (Key et al., 2006) and the normalized difference vegetation index (NDVI) (Rouse et al., 1974). In addition to this, similarity calculation between pre- and post-event data is also popular for feature extraction based on the contrastive learning framework SimCLR (Zhang et al., 2022). It is typically designed for multi-temporal data from satellite platforms and is not suitable for our case. Domain Adaptation is another promising unsupervised approach for burned area mapping (Zhang and Ban, 2023). However, there are only standardized burned areas classification datasets using satellite imagery, which limits the application of Domain Adaptation approaches.

2.2 3D Point Cloud Processing

Even though a quite comprehensive survey on deep-learning-based algorithms for ground filtering has recently been published by Qin et al. (2023), approaches not necessarily based on deep learning are still very popular for 2.5D and 3D laser point processing, because of their absolute metric scales, often higher accuracy, and a scarcer availability of the training data. State-of-the-art conventional methods for point filtering from airborne laser scanning data include volume-based filtering (Piltz et al., 2016; Mousa et al., 2019; Oniga et al., 2023) and hierarchical filtering (Mongus and Žalik, 2012). The recently published Superpoint in RANSAC Planes (SiRP), (Bulatov et al., 2020) approach can be applied to unorganized point clouds to differentiate between 2D manifolds (large and approximately planar surfaces), on the one hand, and 3D and 1D manifolds (chaotic or linear fragments ob the point cloud), on the other hand. Thanks to a pre-processing step similar to voxelization, the method is relatively robust against noise and variable point density and can be applied to both airborne and terrestrial point clouds (Bulatov et al., 2021; Stütz et al., 2023).
We conclude this section with a short review on bushfire severity grading using 3D points. Like us, Kwak et al. (2010) apply combined image and elevation data for two different, strictly speaking jobs. The image data (basically, NDVI) assesses biological damage while the 3D data assesses the physical damage, whereby the Number of Ground Returns and Number of Total Returns were provided by the data capturing software and relied on. Differently to us, it seems that only post-event LIDAR data were available. In (Dixon et al., 2023), the LIDAR-based individual tree detection takes place. Supervised classification of concatenated pre- and post-event images allows establishing which trees are not present anymore. The LIDAR data used were captured a few years before the event. Here, the fact that single tree detection is a cumbersome procedure, the reason why we implemented a more simple, statistical approach.

3. Datasets

A serious bushfire started on 20/12/2019 shortly after 9 am in Cudlee Creek, near Lobethal Town, which is a suburb of Adelaide, the capital of South Australia. The fire, which tragically resulted in the loss of one life, injured 51 firefighters, and destroyed 85 homes[1], also burned 23,295 hectares of land.
For the case study, this paper selected an area of interest (AOI) that includes Bushland Park to analyze the severity of the fire, as shown in Figure 1.

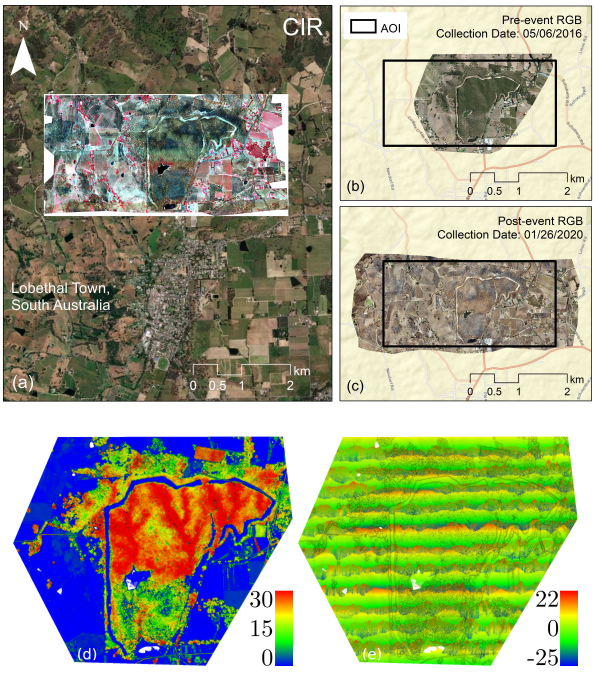

Figure 1. AOI for 2D mapping, defined by the black rectangle. Optical images showcasing (a) post-event Color-Infrared (CIR), (b) pre-event RGB, and (c) post-event RGB data. Pre-event LIDAR data shares the same extent as pre-event RGB data: (d) nDSM in meters, (e) scan angle in degrees.

[1] https://www.cfs.sa.gov.au/about/about/bushfire-history/

3.1 Remote Sensing Data

The dataset for the Bushland Park area is a subset of a larger dataset [2], includes captures from 05/06/2016 (pre-event), 01/26/2020 (less than a month post-event) and 09/09/2020 (over ten months post-event). Data selected for this paper had already been classified using the Airborne Research Australia's (ARA) standard LIDAR- and RGB-imagery-workflow.
The LIDAR scanners and RGB cameras were flown on one of the motorgliders, with the flight conducted at a height of $250\,\mathrm{m}$ AGL around noon before the fire. The post-event flights utilized the LIDAR Q680i-S, Canon 5DMk4 and VNIR hyper-spectral scanner (a modified Specim AISA Eagle 2) at the same flying height. Line spacing was $150\,\mathrm{m}$ on 05/06/2016, and $100\,\mathrm{m}$ on 01/26/2020, and 09/09/2020. CIR data, derived from the hyper-spectral scanner at approximately $0.2\,\mathrm{m}$ ground sampling distance, is only available after the fire and presents healthy, chlorophyll-bearing vegetation as bright red colors. Figure 1 displays the related RGB and CIR data as well as the pre-event LIDAR data.
In addition to aerial imagery acquired from aircraft, we also utilize PlanetScope multi-spectral (MS) data as model inputs, specifically obtaining surface reflectance products (four bands: RGB and NIR) on 12/19/2019 and 01/06/2020.

3.2 Reference Data

Labels of the datasets are generated by aerial photo interpretation, which involves analyzing, processing, and interpreting images collected from aircraft to gather information about bushfire damages. First, we use the initial k-means clustering result of CIR imagery as candidates for labels of burned areas. However, due to the similarities between some water bodies, black ashes after the bushfire, and burned areas, NDVI is calculated from post-event CIR imagery to distinguish roads or water bodies from burned areas. We manually determine the threshold for this NDVI map to reduce the noise and guarantee high recall. Then labels for burned areas can be improved by excluding water bodies and roads. It is noteworthy that, due to the similarity in values of water and roads in the NDVI map, setting an appropriate threshold can aid in effectively extracting both water bodies and roads. Pre-event RGB data, with a spatial resolution of $25\,\mathrm{cm}$, is upsampled to $7.4\,\mathrm{cm}$ using Lanczos resampling to match the spatial resolution of post-event data. The region of interest identified using pre-event RGB imagery is not as extensive as identified from post-event aerial data, which restricts our ability to label accurately over some areas. For such areas, we use PlanetScope pre-event data as complementary considering that $3\,\mathrm{m}$ resolution imagery is enough to facilitate the aerial imagery, to create comprehensive labels. However, because of differences in spatial and temporal resolutions between PlanetScope and airborne data, manual annotation is time-consuming. In order to save time, we randomly selected three test sites for manual interpretation for the evaluation step, and the selected test patches would cover as many types of surfaces as possible.

4. Methodology

In this paper, we propose an effective and efficient end-to-end framework to fast detect burned areas based on an unsupervised machine learning method, which fuses the results from airborne post-event RGB, and CIR data with temporal PlanetScope MS data. These datasets are fed into the UsBA_detection model, which facilitates the generation of detailed mapping to distinguish between burned and unburned areas. Following the classification provided by the UsBA_detection model, the processing of 3D data is undertaken. This step is predicated on the binary classification results from the mapping, enabling further grading of severity within the burned areas. Specifically, it allows for the identification of regions experiencing varying degrees of burn severity, dividing them into categories of either low, medium, high, and very high.

4.1 Model Inputs

The airborne-based raw data requires a few preprocessing steps before it can be fed into our proposed model. For post-event UHR RGB data, we first need to mosaic several captures into on large stitched image. Then, the large RGB data is clipped by the region of interest extracted from CIR data extent to make sure both of them share the exact same locations. We split the refined RGB data into rectangular tiles with $1024\,\mathrm{px} \times 1024\,\mathrm{px}$ size for the semantic segmentation model – UNetFormer (Wang et al., 2022). For post-event UHR CIR data preprocessing, there is no need to partition the imagery into smaller tiles. This data can be directly utilized as input for the clustering segmentation method. Furthermore, both pre- and post-event PlanetScope MS data are downloaded and clipped with the previous region of interest, after which the differenced Normalized Difference Vegetation Index (dNDVI) is calculated, allowing reflection of temporal change information. The LIDAR point clouds are used to compute the absolute burned volume and relative severity. Because they have over $200\,000\,000\,\mathrm{pt}$, we investigate only burned classified areas by 2D analysis. We reduce the resolution of the 2D result to $10\,\mathrm{m} \times 10\,\mathrm{m}$ by downsampling, calculating the mean value for each cell.

4.2 UsBA_detection Based on Image Data

4.2.1 Clustering Module We introduce the UsBA_detection model, an unsupervised approach for burned area mapping via the fusion of airborne UHR data and PlanetScope MS data. It is designed to first use the unique spectral characteristics of post-event UHR CIR data acquired from aircraft. The CIR data, inclusive of the NIR band, is particularly sensitive to vegetation, displaying high reflectance for healthy vegetation. This sensitivity enables the rapid and effective classification between unburned vegetation and burned residues. We employ k-means clustering on the CIR data to segregate the area into color-based clusters. The choice of CIR data is predicated on the capacity of the NIR band to differentiate healthy vegetation from burned remnants accurately. By setting the cluster number to five, our model demonstrates optimal performance in extracting carbonized residues, thereby identifying potential burned area candidates. However, relying solely on post-event data introduces a limitation in capturing change information, leading to potential omissions. For instance, trees that were green in pre-event data and turned to a yellowish hue after the event without complete carbonization, may resemble barren soil in CIR imagery, thus risking misclassification.
To address this problem, we incorporate multitemporal PlanetScope MS data within AOI geographical coordinates. By computing dNDVI and applying both PCA and k-means clustering to the PlanetScope data, we generate additional candidates for the burned area. We further perform upsampling (the nearest neighbor interpolation) on the PlanetScope result (original size: $595\,\mathrm{px} \times 1193\,\mathrm{px}$) to match the resolution of the airborne CIR clustering segmentation result (final size: $9791\,\mathrm{px} \times 19\,619\,\mathrm{px}$), ensuring uniformity when fusing.

[2] https://www.airborneresearch.org.au/fires2020

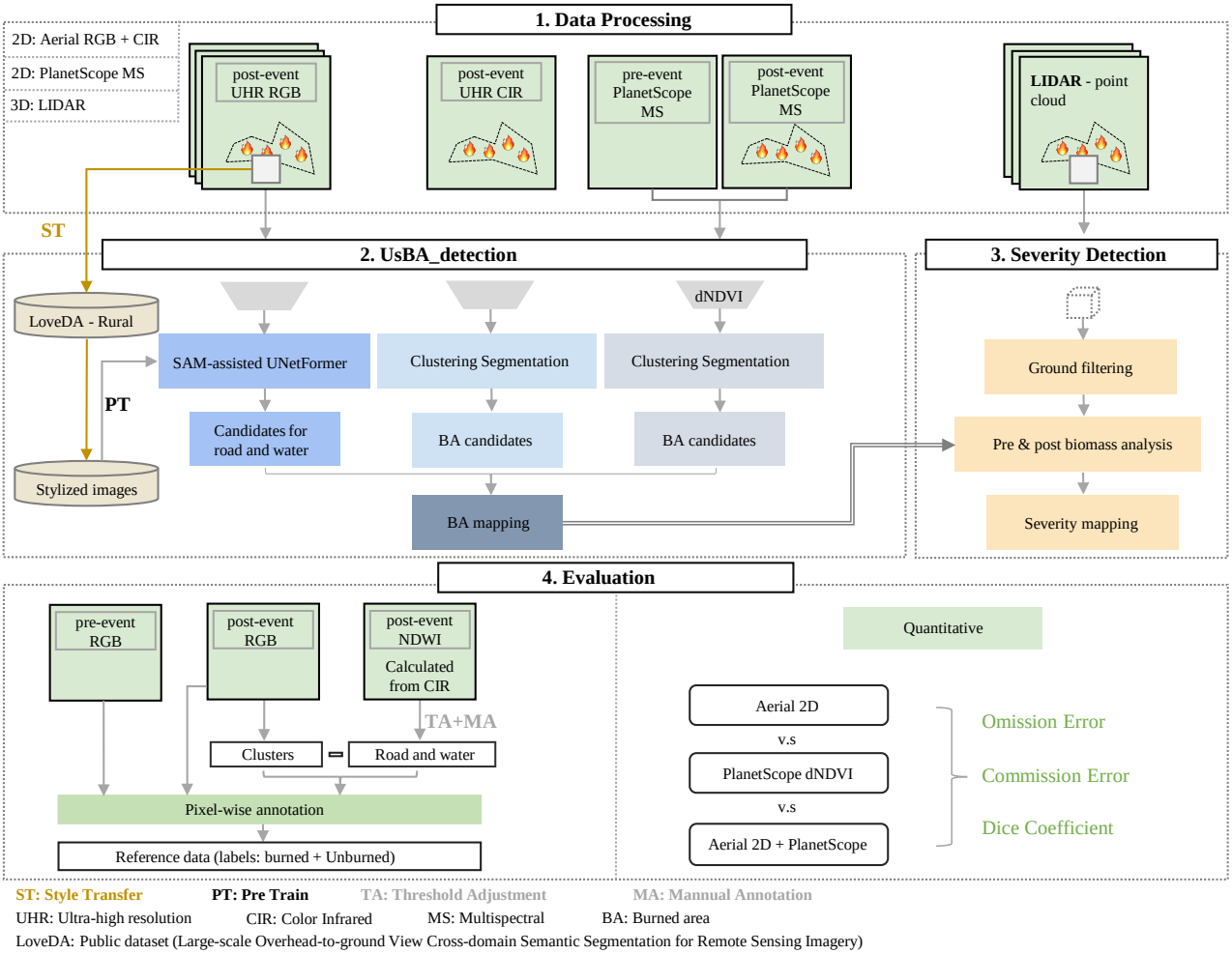

Figure 2. Overview of our pipeline for two-step burn severity mapping. UsBA_detection is the proposed 2D model for burned area mapping, and severity detention utilizes LIDAR data for damage grading.

4.2.2 Refinement Module However, the integration of candidates from both datasets still introduces potential interference from water bodies and roads, which share similar color characteristics with carbonized residues in CIR data.

To refine our mapping, we employ the SAM-assisted semantic segmentation model (Ma et al., 2023) to accurately delineate water bodies and roads using post-event airborne RGB data. The SAM model is famous for its precise segmentation boundaries, enhancing the performance of the semantic segmentation models. In our work, UNetFormer (Wang et al., 2022) is chosen for its semantic segmentation capabilities and the segmentation result is improved by the object boundaries generated via SAM. We pre-train the UNetFormer model on the LoveDA dataset of Wang et al. (2021), which includes ground truth labels with 7 categories: *building, road, water, barren, forest, agriculture, and background*. Due to the bias of the different datasets, the pre-trained UNetFormer may not perform well on our RGB dataset. To alleviate this issue, the style transfer (Huang and Belongie, 2017) is applied to generate target-style images by treating the given one unlabeled target image ($1024\,\mathrm{px} \times 1024\,\mathrm{px}$, split tile from post-event RGB imagery) as an “anchor style”. This transformation normalizes the source images (LoveDA Rural) based on their mean and standard deviation, and then adjusts them using the target’s mean and standard deviation, which are recalculated to include statistic offsets controlled by weights sampled from a Gaussian distribution $\mathcal{G}(0, 1)$. We pre-train the SAM-assisted UNetFormer on the target-style dataset, using it to obtain and downsample masks for water bodies and roads to match CIR spatial resolution. Finally, we exclude water bodies and roads from combined burned area candidates.

A binary classification map is the output of UsBA_detection model, distinguishing between burned and unburned areas. It is fed into the biomass analysis module for further analysis.

4.3 Severity Detection Based on 3D

4.3.1 Ground Filtering We start by retrieving the ground map, applying the previously developed SiRP method to the point cloud X. This method, briefly described here for completeness and referred to in (Bulatov et al., 2020, 2021; Stütz et al., 2023) for a more detailed explanation, presupposes grouping the points into voxel-like structures called superpoints (SP) V, whereby V has not only a geographic coordinate but also a subset X_V of the original point set assigned to it. For each of these SP V, the dominant plane is computed using the points in X_V and the well-known RANSAC algorithm (Fischler and Bolles, 1981). Those superpoints, which are not inliers of their planes, are set to inactive. This result is refined using a clustering method whereby superpoints forming too small clusters are set to inactive as well. Inactive SP are supposed to be those

This contribution has been peer-reviewed. The double-blind peer-review was conducted on the basis of the full paper.
https://doi.org/10.5194/isprs-annals-X-4-2024-29-2024 | © Author(s) 2024. CC BY 4.0 License.

lying in vegetation regions, while clustering results may mean some occasionally planar regions, such as tree crones. Finally, for each point $x \in X$, we take the corresponding superpoint and a few neighboring ones (in the sense of k nearest neighbors). From the information about how many RANSAC-planes corresponding to active SP x is inlier of, we decide whether x is a ground point.

4.3.2 Burn Severity Mapping In the next step, we compute the biomass loss. To speed up computation, we only investigate areas, classified as burned in the 2D step. We voxelize the non-ground-points in pre- and post-event ALS point clouds. The voxel size r must be higher than possible displacements caused by wind. Contrarily, a *cell* has a dimension of several meters (in our case: $10\,\mathrm{m}$) and signifies the relevant for damage assessment area. For each cell, we count the number of voxels that have been filled in pre- but not in post-event point cloud. The absolute ($\#B \cdot r^3$) and relative ($\#B/\#V$) measures, whereby $\#V$ is the total number of voxels in the cell, are used to assess the results on upsampling burning area mapping.

5. Results

To assess the accuracy of 2D burned area mapping (Section 5.1, we use Omission Error (OE), Commission Error (CE), and Dice Coefficient (DC), calculated from True Positive (TP), False Positive (FP), True Negative (TN), and False Negative (FN) values in a confusion matrix (Padilla et al., 2015). For 3D burn severity mapping, we subdivide the corresponding section 5.2 into two parts. Namely, in Section 5.2.1, we evaluate our ground filtering method using LAStools (LAStools, 2022) as the reference data, since it is an industrial standard tool. Due to the absence of reference data on burn severity levels, our evaluation will be limited to qualitative assessment (Section 5.2.2).

5.1 Burned Area Mapping

According to our observation that burned area candidates derived from the clustering results of CIR data and PlanetScope dNDVI incorrectly classified water bodies and roads as burned areas, we have incorporated a refinement module to mitigate interference from these two types of objects, thereby enhancing the performance of our 2D burn mapping results. As shown in Figure 3, the pre-trained UNetFormer, assisted by SAM, exhibits satisfactory performance on post-event RGB data, especially in segmenting these two categories: water and roads, demonstrating a superiority over the segmentation of other categories and fulfilling the requirements of our unsupervised model.

As mentioned before, some sites (site 1: $1705\,\mathrm{px} \times 1187\,\mathrm{px}$; site 2: $1691\,\mathrm{px} \times 1201\,\mathrm{px}$; site 3: $831\,\mathrm{px} \times 518\,\mathrm{px}$) are chosen for manual labeling, and the accuracy of the burned area mapping is assessed for these sites. We experiment with different input data sources, which include PlanetScope MS imagery, aerial CIR + RGB data, and fusion of PlanetScope and aerial 2D data. Figure 4 provides an overview of their prediction maps. Our UsBA_detection model, solely based on aerial 2D data, tends to exhibit more detailed and extensive burned areas than the dNDVI baseline (dNDVI + PCA) derived from PlanetScope data. By combining aerial 2D with PlanetScope data, this model achieves more accurate segmentation of burned areas.

The quantitative analysis results computed for the burned area detection are presented in Table 1. For the PlanetScope data, the dNDVI + PCA method results in the worst OE of 25.0% and DC of 85.1%. Our model solely using aerial 2D data achieves better DC (87.4%) with a reduced OE (21.0%), indicating its proficient capability in accurately identifying burned areas. More outstanding improvements in DCs of fusion inputs are observed over every case site. Moreover, our model with the combination of Aerial 2D and PlanetScope data considerably improves the detection of burned areas, reducing omission errors and increasing the accuracy of detection correctness compared to using each data source individually. (Total OE: 9.0%; total CE: 2.8%; total DC: 94%).

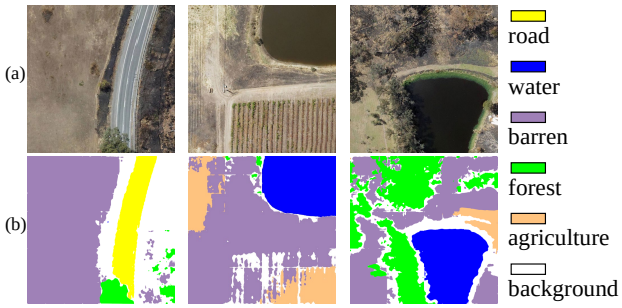

Figure 3. Semantic segmentation results based on SAM-assisted UNetFormer. The model has been pre-trained on target-style rural LoveDA dataset. (a) post-event RGB tiles ($1024\,\mathrm{px}$); (b) corresponding semantic segmentation results.

Data	Method	Site	OE	CE	DC
PlanetScope	dNDVI + PCA	1	21.1%	0.7%	87.9%
		2	28.6%	2.2%	82.6%
		3	25.3%	0.8%	85.2%
		Total	25.1%	**1.3%**	85.1%
Aerial 2D	Ours	1	24.5%	2.2%	84.3%
		2	19.5%	0.3%	89.1%
		3	17.5%	4.2%	88.7%
		Total	21.0%	1.7%	87.4%
Aerial 2D + PlanetScope	Ours	1	11.4%	2.4%	92.9%
		2	7.4%	1.9%	95.2%
		3	8.1%	4.2%	93.8%
		Total	**8.9%**	2.3%	**94.3%**

Table 1. Quantitative analysis results for burned area mapping using different datasets.

5.2 Analysis of 3D data

5.2.1 Ground Filtering: Assessment of SiRP The result of evaluation using LAStools as the reference looks promising, with an overall accuracy of around $90\,\%$ in the confusion matrices in Figure 5. It is comparable to the previous works, such as of Bulatov et al. (2021). Qualitatively, LAStools and SiRP correctly classify points that are clearly soil or high vegetation. However, there are noticeable differences, especially in grass-covered fields (Figure 5, top). SiRP allows for greater unevenness in the ground, which results in low vegetation often being classified as ground. This key difference is evident in the confusion matrices in Figure 5. In the forest, this behavior is also observed (Figure 5, bottom). Comparing the confusion matrices, one notes that the best result of ground filtering is obtained immediately after the bushfire on 01/26/2020, because the fire destroys a lot of low and medium vegetation. Conversely, after new vegetation grows, the performance of SiRP regarding reference

This contribution has been peer-reviewed. The double-blind peer-review was conducted on the basis of the full paper.
https://doi.org/10.5194/isprs-annals-X-4-2024-29-2024 | © Author(s) 2024. CC BY 4.0 License.

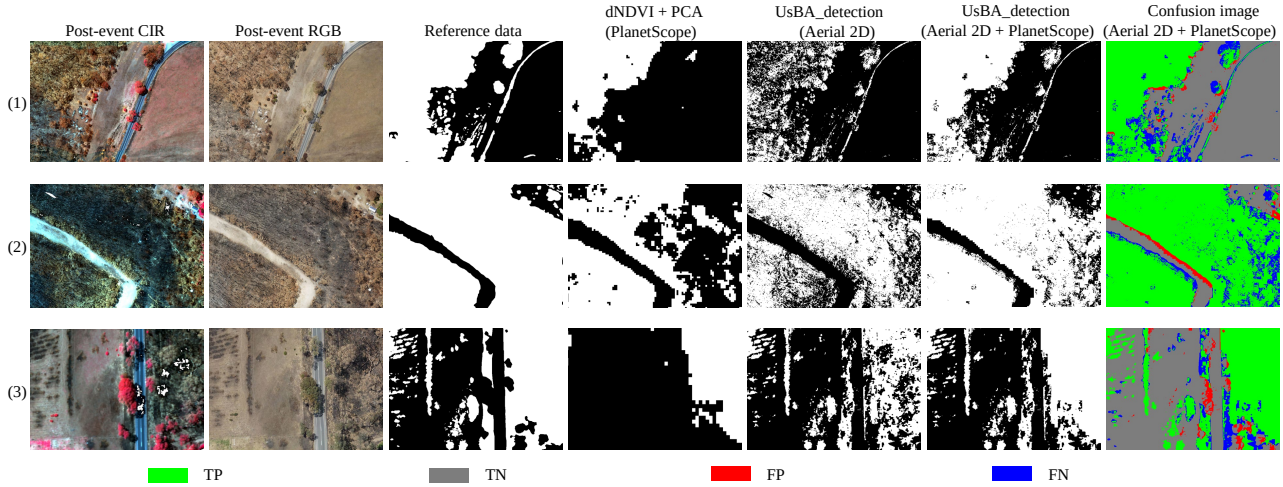

Figure 4. Comparison of 2D prediction results for burned area mapping using different datasets. The final column is confusion images for our model prediction results using aerial 2D and PlanetScope data.

provided by LAStools degrades again (shown in confusion matrix on 09/09/2020, Figure 5).

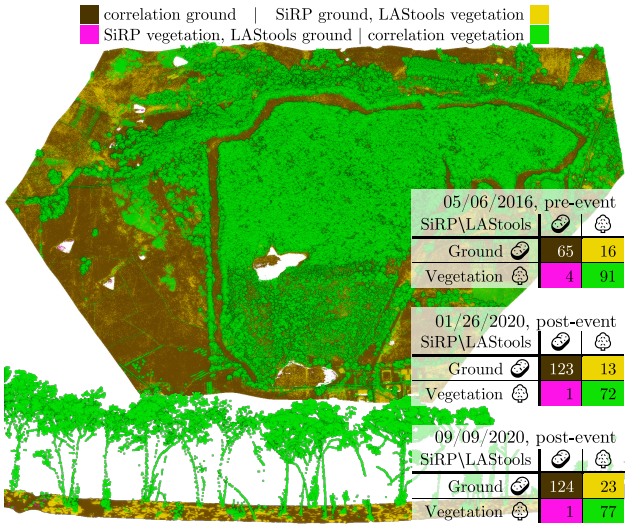

Figure 5. Confusion matrix comparison of ground filtering, with number of points in millions; Qualitative evaluation with images from 09/09/2020 (post-event): Top: Nadir view, bottom: side view.

5.2.2 Burn Severity Mapping As no change in volume is to be expected for the ground, we remove the corresponding points from future analysis. The ash produced by a fire should also not be included in the volume difference. Therefore, we consider it useful to use the ability of SiRP to remove soil and low vegetation in order to obtain exactly the volume of the large plants, which make up the majority of the biomass in the forest. We note that the biggest obstacle on the way to an objective damage grading is that the only pre-event data was taken four years and not immediately before the event. During this time, vegetation is very likely to be subject to many changes. Actually, Dixon et al. (2023) have mentioned a threshold of three years. Thus, we can only provide a *lower bound* on the burn severity by comparing the biomass using the method of Section 4.3.2 because we basically estimate what is lacking in 2020 compared to 2016.

Following Hosseini and Lim (2022) and Tehrany et al. (2021), damage is classified both in absolute and relative terms in five classes, as depicted in the tables within Figure 6. The entire area exhibits medium to severe relative destruction ($> 25\,\%$), as shown in Figure 6a, with only a few instances of minor destruction ($\leq 25\,\%$). Particularly, the southern part of the area is characterized by severe destruction, predominantly due to the prevalence of medium vegetation, which is particularly susceptible to fire damage. Conversely, the lower degree of destruction observed in the northern half of the area can be attributed to the presence of a large stand of trees, which exhibited greater resilience to the fire. This observation supports the application of the SiRP methodology, as, without it, regions characterized solely by low vegetation would appear to sustain a high degree of relative destruction, despite contributing minimally to the overall volume of destroyed biomass.
While considering the absolute volume of destruction, as depicted in Figure 6b, the focus shifts to the northern area where the forest is significantly taller compared to the southern part. Notably, there is an east-west pattern in the results, where destruction is consistently higher. This pattern is a result of data collection method (shown in Figure 1d), since the laser penetration of vegetation varies depending on the scan angle. Nevertheless, the results align well with the fire zone analysis. The lighter areas in the southern part correspond to lower volume loss. Along the forest aisle, heavy destruction is nearly continuous due to the dense undergrowth and increased fire intensity at the forest edge.
In summary, the fire has a significant impact, resulting in the destruction of around $3\,000\,000\,\mathrm{m}^3$ of biomass. On average, this represents a $68\,\%$ loss of biomass. These numbers include fire destruction and biomass removed during possible post-fire cleanup operations until 09/09/2020.

6. Conclusion

Fire is a major degradation component for the vegetation and forests, not only threatening the bio-diversity and human lives, but also contributing to significant emissions of carbon dioxide. Once such a bushfire happened, all available sensors have to be employed to assess the damage and provide decision-makers a picture of the situation as quickly as possible and as comprehensively as necessary so that they can determine their

This contribution has been peer-reviewed. The double-blind peer-review was conducted on the basis of the full paper.
https://doi.org/10.5194/isprs-annals-X-4-2024-29-2024 | © Author(s) 2024. CC BY 4.0 License.

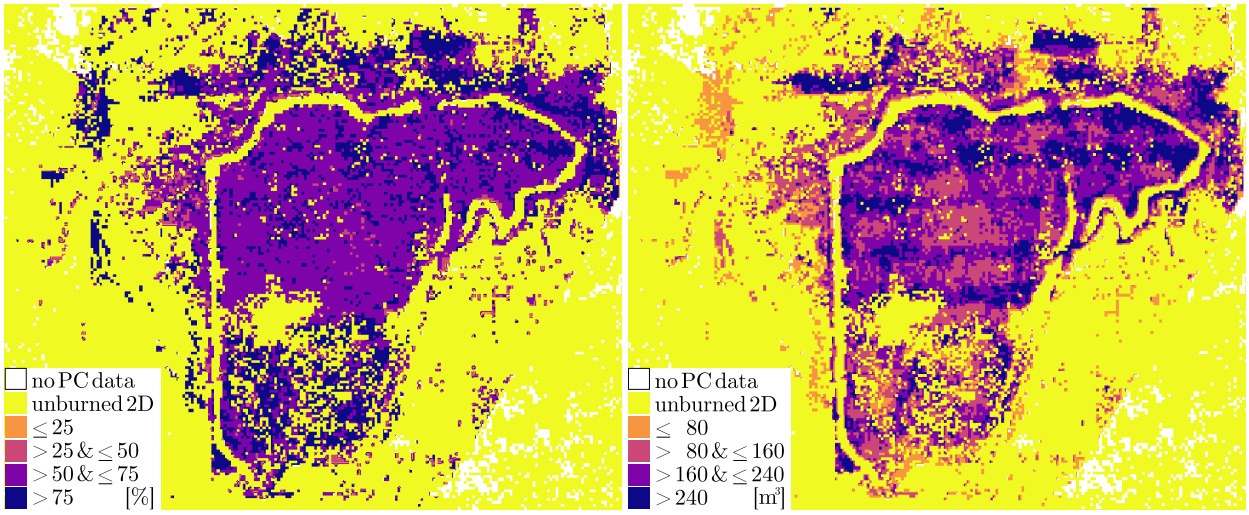

(a) percent (b) volume in cubic meters

Figure 6. Immediate fire damage on 01/26/2020 vs. 05/06/2016. Pixel size is 10 m × 10 m. PC is an abbreviation for point cloud.

options for action. In this paper, a combined 2D/3D pipeline for assessing the burn severity is proposed. In 2D, the newly developed UsBA_detection model takes as input bi-temporal medium-resolution PlanetScope data and post-event UHR aerial imagery to identify regions for burn severity analysis. This model encompasses a clustering module and a refinement module for enhanced performance, and the mapping results demonstrate the effectiveness of UsBA_detection model and showcase the utility of combined use of data for burned area mapping with improved OEs, CEs, and DCs. In 3D, the hypothesized burned areas are analyzed regarding biomass loss. We first perform ground filtering using the already available implementation of SiRP method and then grade the damage severity using a straightforward approach based on change detection.

The advantage of the proposed methodology is that no training data has to be collected. However, three conceptual limitations and areas for improvement have been identified: 1) In 2D, impact of shadows caused some false positives while there were some missed detections of white ash. 2) In 3D, the pre-event data might not be available, and even if it is, it may be so outdated that merely a lower bound on biomass change can be provided because a lot of vegetation could have grown in the meantime. 3) The primary limitation is that spuriously detected water bodies and roads are not analyzed by the 3D approach as we process 2D and 3D data using a loosely connected approach to prevent an explosion in the number of network parameters. We are conscious that the current research trends focus more and more on the early fusion of data stemming from different sensors – because different data sources could complement each other and cope with each other’s insufficiencies. Therefore, future research could beneficially explore the integration of 3D data into a semi-supervised or unsupervised deep learning pipeline that utilizes optical imagery. This integration, potentially through the generation of an additional layer, represents a promising extension of the approach presented herein.

References

Arkin, J., Coops, N. C., Hermosilla, T., Daniels, L. D., Plowright, A., 2019. Integrated fire severity–land cover mapping using very-high-spatial-resolution aerial imagery and point clouds. *International Journal of Wildland Fire*, 28(11), 840–860.

Bai, T., Ge, L., Sepasgozar, S. M. E., Sheng, Z., Liu, C., Wu, Y., Zhang, Q., 2023. An improved luminance contrast saliency map for burned area mapping based on insar coherence difference image. *IGARSS 2023 - 2023 IEEE International Geoscience and Remote Sensing Symposium*, 7198–7201.

Belenguer-Plomer, M. A., Tanase, M. A., Chuvieco, E., Bovolo, F., 2021. CNN-based burned area mapping using radar and optical data. *Remote Sensing of Environment*, 260, 112468.

Bulatov, D., Stütz, D., Hacker, J., Weinmann, M., 2021. Classification of airborne 3D point clouds regarding separation of vegetation in complex environments. *Applied Optics*, 60(22), F6–F20.

Bulatov, D., Stütz, D., Lucks, L., Weinmann, M., 2020. Superpoints in RANSAC planes: A new approach for ground surface extraction exemplified on point classification and context-aware reconstruction. *Proc. Int. Conf. on Compute Graphics Theory and Applications*, 25–37.

Cho, A. Y., Park, S.-e., Kim, D.-j., Kim, J., Li, C., Song, J., 2022. Burned area mapping using Unitemporal Planetscope imagery with a deep learning based approach. *IEEE Journal of Selected Topics in Applied Earth Observations and Remote Sensing*, 16, 242–253.

Chuvieco, E., Mouillot, F., van der Werf, G. R., San Miguel, J., Tanase, M., Koutsias, N., García, M., Yebra, M., Padilla, M., Gitas, I., Heil, A., Hawbaker, T. J., Giglio, L., 2019. Historical background and current developments for mapping burned area from satellite Earth observation. *Remote Sensing of Environment*, 225, 45-64.

Davey, S. M., Sarre, A., 2020. Editorial: the 2019/20 Black Summer bushfires. *Australian Forestry*, 83(2), 47-51. https://doi.org/10.1080/00049158.2020.1769899.

Dixon, D. J., Zhu, Y., Brown, C. F., Jin, Y., 2023. Satellite detection of canopy-scale tree mortality and survival from California wildfires with spatio-temporal deep learning. *Remote Sensing of Environment*, 298, 113842.

Fischler, M. A., Bolles, R. C., 1981. Random Sample Consensus: A Paradigm for Model Fitting with Applications to Image Analysis and Automated Cartography. *Commun. ACM*, 24(6), 381–395.

Gibson, R., Danaher, T., Hehir, W., Collins, L., 2020. A remote sensing approach to mapping fire severity in south-eastern Australia using sentinel 2 and random forest. *Remote sensing of environment*, 240, 111702.

Hosseini, M., Lim, S., 2022. Gene expression programming and data mining methods for bushfire susceptibility mapping in New South Wales, Australia. *Natural Hazards*, 113(2), 1349–1365.

Hu, X., Zhang, P., Ban, Y., 2023. Large-scale burn severity mapping in multispectral imagery using deep semantic segmentation models. *ISPRS Journal of Photogrammetry and Remote Sensing*, 196, 228–240.

Huang, X., Belongie, S., 2017. Arbitrary style transfer in real-time with adaptive instance normalization. *Proceedings of the IEEE international conference on computer vision*, 1501–1510.

Key, C. H., Benson, N. C. et al., 2006. FIREMON: Fire Effects Monitoring and inventory system, Landscape assessment (LA). Technical Report Gen. Tech. Rep. RMRS-GTR-164., US Department of Agriculture, Forest Service, Rocky Mountain Research.

Kwak, D.-A., Chung, J., Lee, W.-K., Kafatos, M., Lee, S. Y., Cho, H.-K., Lee, S.-H., 2010. Evaluation for damaged degree of vegetation by forest fire using Lidar and a digital aerial photograph. *Photogrammetric Engineering & Remote Sensing*, 76(3), 277–287.

LAStools, 2022. Efficient LIDAR Processing Software. http://rapidlasso.com/LAStools.

Lizundia-Loiola, J., Otón, G., Ramo, R., Chuvieco, E., 2020. A spatio-temporal active-fire clustering approach for global burned area mapping at 250 m from MODIS data. *Remote Sensing of Environment*, 236, 111493.

Ma, X., Wu, Q., Zhao, X., Zhang, X., Pun, M.-O., Huang, B., 2023. SAM-Assisted remote sensing imagery semantic segmentation with object and boundary constraints. *arXiv preprint arXiv:2312.02464*.

McKenna, P., Erskine, P. D., Lechner, A. M., Phinn, S., 2017. Measuring fire severity using UAV imagery in semi-arid central Queensland, Australia. *International Journal of Remote Sensing*, 38(14), 4244–4264.

Mongus, D., Žalik, B., 2012. Parameter-free ground filtering of LiDAR data for automatic DTM generation. *ISPRS Journal of Photogrammetry and Remote Sensing*, 67, 1 - 12.

Mousa, Y. A., Helmholz, P., Belton, D., Bulatov, D., 2019. Building detection and regularisation using DSM and imagery information. *Photogrammetric Record*, 34(165), 85–107.

Oniga, V.-E., Loghin, A.-M., Macovei, M., Lazar, A.-A., Boroianu, B., Sestras, P., 2023. Enhancing LiDAR-UAS derived digital terrain models with hierarchic robust and volume-based filtering approaches for precision topographic mapping. *Remote Sensing*, 16(1), 78.

Padilla, M., Stehman, S. V., Ramo, R., Corti, D., Hantson, S., Oliva, P., Alonso-Canas, I., Bradley, A. V., Tansey, K., Mota, B., Pereira, J. M., Chuvieco, E., 2015. Comparing the accuracies of remote sensing global burned area products using stratified random sampling and estimation. *Remote Sensing of Environment*, 160, 114-121.

Piltz, B., Bayer, S., Poznanska, A.-M., 2016. Volume based DTM generation from very high resolution photogrammetric DSMs. *International Archives of the Photogrammetry, Remote Sensing and Spatial Information Sciences*, 41, 83–90.

Qin, N., Tan, W., Ma, L., Zhang, D., Guan, H., Li, J., 2023. Deep learning for filtering the ground from ALS point clouds: A dataset, evaluations and issues. *ISPRS Journal of Photogrammetry and Remote Sensing*, 202, 246–261.

Ramo, R., Chuvieco, E., 2017. Developing a random forest algorithm for MODIS global burned area classification. *Remote Sensing*, 9(11), 1193.

Roteta, E., Bastarrika, A., Padilla, M., Storm, T., Chuvieco, E., 2019. Development of a Sentinel-2 burned area algorithm: Generation of a small fire database for sub-Saharan Africa. *Remote Sensing of Environment*, 222, 1–17.

Rouse, J. W., Haas, R. H., Schell, J. A., Deering, D. W. et al., 1974. Monitoring vegetation systems in the Great Plains with ERTS. *NASA Spec. Publ*, 351(1), 309.

Roy, D. P., Huang, H., Boschetti, L., Giglio, L., Yan, L., Zhang, H. H., Li, Z., 2019. Landsat-8 and Sentinel-2 burned area mapping - A combined sensor multi-temporal change detection approach. *Remote Sensing of Environment*, 231, 111254.

Sharples, J. J., Cary, G. J., Fox-Hughes, P., Mooney, S., Evans, J. P., Fletcher, M.-S., Fromm, M., Grierson, P. F., McRae, R., Baker, P., 2016. Natural hazards in Australia: extreme bushfire. *Climatic Change*, 139(1), 85-99.

Stütz, D., Li, J., Huai, J., Bulatov, D., 2023. Ground filtering of co-registered mobile and stationary laser scans by using superpoints in RANSAC planes. *ISPRS Annals of the Photogrammetry, Remote Sensing and Spatial Information Sciences*, 10, 589–596.

Tehrany, M. S., Özener, H., Kalantar, B., Ueda, N., Habibi, M. R., Shabani, F., Saeidi, V., Shabani, F., Touhafi, A., 2021. Application of an ensemble statistical approach in spatial predictions of bushfire probability and risk mapping. *Journal of Sensors*, 2021, 6638241.

Wang, J., Zheng, Z., Ma, A., Lu, X., Zhong, Y., 2021. LoveDA: A remote sensing land-cover dataset for domain adaptive semantic segmentation. *Proceedings of the Neural Information Processing Systems Track on Datasets and Benchmarks*, 1.

Wang, L., Li, R., Zhang, C., Fang, S., Duan, C., Meng, X., Atkinson, P. M., 2022. UNetFormer: A UNet-like transformer for efficient semantic segmentation of remote sensing urban scene imagery. *ISPRS Journal of Photogrammetry and Remote Sensing*, 190, 196-214.

Zhang, B., Wang, H., Alabri, A., Bot, K., McCall, C., Hamilton, D., Ružička, V., 2022. Unsupervised wildfire change detection based on contrastive learning. *arXiv preprint arXiv:2211.14654*.

Zhang, P., Ban, Y., 2023. Unsupervised geospatial domain adaptation for large-scale wildfire burned area mapping using Sentinel-2 MSI and Sentinel-1 SAR data. *IGARSS 2023-2023 IEEE International Geoscience and Remote Sensing Symposium*, 5742–5745.

Zhang, Q., Ge, L., Zhang, R., Metternicht, G. I., Du, Z., Kuang, J., Xu, M., 2021. Deep-learning-based burned area mapping using the synergy of Sentinel-1&2 data. *Remote Sensing of Environment*, 264, 112575.